

## Direct Numerical Simulation of a Counter-Rotating Vortex Pair Embedded in Turbulence

W. Rojanaratanangkule<sup>1</sup> and J. Tunkaew<sup>1</sup>

<sup>1</sup>Department of Mechanical Engineering  
Chiang Mai University, Chiang Mai 50200, Thailand

### Abstract

Direct numerical simulations are performed to investigate the effect of the ambient turbulence on the evolution and instability of a counter-rotating vortex pair. The external turbulence is modelled as homogeneous isotropic turbulence with intensity of 7%. The ambient turbulence alters the most amplified mode from the short-wavelength elliptic to the long-wavelength Crow mode. The Crow instability gives rise to the two-vortex mutual interaction, resulting in the transformation of the vortex pair into an array of vortex rings.

### Introduction

A counter-rotating vortex pair is one of the fascinating flow models for engineers and physicists due to its relevance to a wake of an aircraft. Such wake vortices are large, long-lived and possess a strong circulation [12]. The occurrence of these wake vortices can be hazardous to the following aircraft since it may cause the loss of altitude. For a safety reason, the following aircraft has to wait until the wake vortices disappear which may result in the flight delay [3]. Thus, obtaining the better understanding of the dynamics of a counter-rotating vortex pair, especially in a realistic environment (e.g. stratified or turbulent background), is important to predict the behaviour of the aircraft wake vortices.

In a quiescent background, it is well known that the vortex pair undergoes transition via two types of three-dimensional instability, namely the short-wavelength elliptic and long-wavelength Crow instabilities (see e.g. [6]). Both instabilities develop in the same manner in which the vortex pair axially deforms into a sinusoidal shape but with different dominant wavelength. When the Crow mode is dominant, the most amplified wavelength is relatively long compared to the initial vortex separation distance ( $b_0$ ). The linear instability analysis of Crow [2] predicted that the most amplified wavelength is  $8.6b_0$ , while the flight tests of Chevalier [1] found that the most amplified wavelength varies from  $5b_0$  to  $10b_0$  in weak atmospheric turbulence. The Crow instability results in the vortex reconnection that leads to the occurrence of a chain of vortex rings. These large-scale vortical structures can persist for very long times. On the other hand, the elliptic instability causes the vortex pair to distort with very short wavelength of about  $b_0$  [7, 5, 9]. The elliptic mode also induces the appearance of the transverse secondary vortex, which results in the fast breakdown to turbulence and the rapid decay of the vortex pair.

In a realistic environment, the vortex pair can be interacted with and affected by various backgrounds in which it can exist (e.g. rotating, stably stratified or turbulent background). In a weakly to moderately stably stratified fluid ( $\infty \geq Fr \geq 2$ , where  $Fr$  being the Froude number), the stratification may reduce the vortex separation distance without changing the type of the instability. This leads to the earlier transition and higher growth rate [9]. The elliptic mode may be altered to the Crow mode when the stratification is strong ( $Fr < 2$ ) [11]. The effect of the ambient turbulence seems to be more pronounced than that of the stratification. The earlier onset and the reconnection process

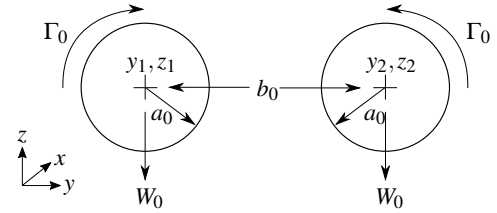


Figure 1. Schematic of the counter-rotating vortex.

are observed when the vortex pair is influenced by the external turbulence. Additionally, the decay rate of the vortex pair was found to increase [11].

The aim of this work is to study the evolution of the vortex pair subject to external turbulence in the background. The focus is on how the ambient turbulence affects the instabilities of the vortex pair, the most amplified mode and its growth rate. Two cases, namely the vortex pair in a quiescent fluid and in ambient turbulence with intensity of 7%, are investigated.

### Numerical Approach

In this study, we consider a counter-rotating vortex pair of core radius  $a$  and separation distance  $b$ , with circulation  $\Gamma$  and descent velocity  $W = \Gamma/2\pi b$ . The vortex pair propagates along the  $x$ -direction of the Cartesian coordinate  $x_i = (x, y, z)$  whose corresponding velocity is  $u_i = (u, v, w)$  (see figure 1). The vortex pair is generated in such a way that the initial centre of each vortex is located at  $(y_1, z_1)$  and  $(y_2, z_2)$ . The equations governing the flow are the continuity and incompressible Navier–Stokes equation written in tensor notation as,

$$\frac{\partial u_i}{\partial x_i} = 0, \quad (1)$$

$$\frac{\partial u_i}{\partial t} + \frac{\partial u_i u_j}{\partial x_j} = -\frac{1}{\rho} \frac{\partial p}{\partial x_i} + \nu \frac{\partial^2 u_i}{\partial x_j \partial x_j}, \quad (2)$$

where  $t$  denotes time,  $p$  is the pressure,  $\rho$  and  $\nu$  are respectively the fluid density and kinematic viscosity. The second-order explicit Adams–Bashforth scheme is used for the temporal integration, while the spatial derivatives are performed on a staggered grid using a second-order central finite-difference scheme. The divergence-free condition is obtained via a standard pressure-projection method. A multigrid method is employed to solve the resulting Poisson equation for the pressure. The simulations of the vortex pair in a quiescent and turbulent background are conducted in a triply periodic box of size  $6\pi \times 2\pi \times 6\pi$  with the grid resolution of  $384 \times 128 \times 384$ . It should be noted that the domain length in the axial direction ( $x$ ) is long enough to represent the characteristic of the Crow instability, while that in the transverse direction ( $z$ ) is sufficient large that the effect of periodicity is negligible. The height of the computational domain is chosen in such a way that it can accumulate the whole breakdown process of the vortex pair before it reaches the bottom of the domain. The time step used in this

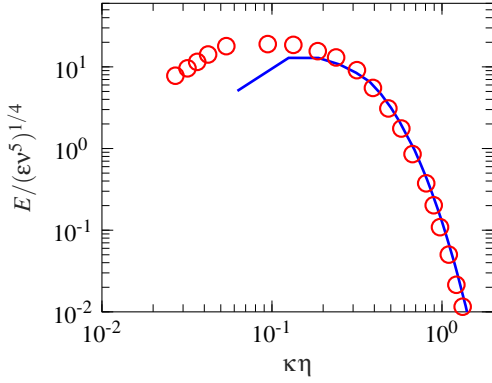


Figure 2. Three-dimensional energy spectrum normalised in Kolmogorov variables: — Present,  $Re_\lambda = 11.65$ ;  $\circ$  Mansour & Wray [8],  $Re_\lambda = 15.7$ .

work is  $\Delta T = 2.5 \times 10^{-3}$ , that provides the maximum Courant–Friedrichs–Lewy (CFL) number, based on the local maximum velocity and grid size, always less than 0.25.

#### Counter-Rotating Vortex Pair

The Lamb–Oseen vortex is used to represent the counter-rotating vortex pair as in the previous numerical works [5, 9] since it fits well with the experiment about the instabilities of the vortex pair of Leweke & Williamson [7]. The axial vorticity distribution ( $\omega_x$ ) is defined as,

$$\omega_{x,0}(y,z) = \frac{\Gamma_0}{\pi a_0^2} \exp\left[-\frac{(y-y_1)^2 + (z-z_1)^2}{a_0^2}\right] - \frac{\Gamma_0}{\pi a_0^2} \exp\left[-\frac{(y-y_2)^2 + (z-z_2)^2}{a_0^2}\right], \quad (3)$$

where the subscript 0 indicates the initial value. The initial vortex aspect ratio  $a_0/b_0 = 0.177$  and the circulation Reynolds number  $Re_\Gamma = \Gamma_0/\nu = 2400$  are chosen to be close to the experiment [7]. To allow the three-dimensional instabilities develop naturally, we follow Orlandi *et al.* [10] by introducing the random perturbation of the velocity field with the amplitude of  $0.027W_0$  to the region of the vortex core.

#### Vortex Pair in Ambient Turbulence

In the present study, the ambient turbulence is modelled as the homogeneous isotropic turbulence (HIT). To obtain the desired turbulence intensity  $Tu = u'/W_0 = 7\%$  ( $u'$  being the streamwise velocity fluctuation) the pre-simulation of the decaying HIT is conducted. Note that the turbulence intensity considered in this work is moderate compared to the atmospheric ambient turbulence [13]. For this pre-simulation, the initial solenoidal velocity field is generated in the spectral space satisfying the following spectrum

$$E_0(\kappa) = \frac{q^2 \kappa^\sigma}{2A \kappa_p^{\sigma+1}} \exp\left[-\frac{\sigma}{2} \left(\frac{\kappa}{\kappa_p}\right)^2\right], \quad (4)$$

$$A = \int_0^\infty \frac{\kappa^\sigma}{\kappa_p^{\sigma+1}} \exp\left[-\frac{\sigma}{2} \left(\frac{\kappa}{\kappa_p}\right)^2\right] d\kappa, \quad (5)$$

where  $\sigma = 4$ ,  $\kappa_p = 9$ ,  $q^2 = 3$  and  $\kappa = (\kappa_i \kappa_j)^{1/2}$  is the wavenumber magnitude. The pre-simulation of the ambient turbulence is allowed to evolve as a decaying HIT until the desired tur-

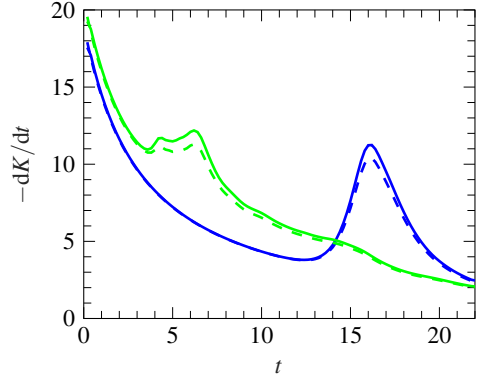


Figure 3. History of rate of change of volume-integrated kinetic energy,  $-dK/dt$  (—), and volume-integrated rate of kinetic energy dissipation,  $\epsilon_K$  (---), for  $Tu = 0$  (blue) and  $Tu = 7\%$  (green).

bulence intensity is achieved. At  $Tu = 7\%$ , the microscale Reynolds number  $Re_\lambda = u'\lambda/\nu$  is about 11.65 ( $\lambda$  being the Taylor microscale), while the streamwise integral length scale  $L_{11}$  is about 0.74. Figure 2 shows that the three-dimensional energy spectrum at this turbulence intensity agrees reasonably well with that of Mansour & Wray [8] at  $Re_\lambda = 15.7$  except in the region of large scales due to the discrepancy in the microscale Reynolds number. The external turbulent field is then superimposed onto the outer region of the vortex pair.

#### Results

In this section, the results from direct numerical simulation (DNS) of the vortex pair in the quiescent and turbulent backgrounds are presented. First, the check of the adequacy of the grid resolution used is performed. Then, the effect of background turbulence on the instability of the vortex pair is analysed.

#### Resolution Check

The adequacy of the grid resolution used can be verified by comparing the balance of the volume-integrated instantaneous kinetic energy  $K$  equation written as

$$\frac{dK}{dt} = -\epsilon_K, \quad (6)$$

where  $\epsilon_K$  is the volume-integrated rate of kinetic energy dissipation. The history of  $-dK/dt$  and the dissipation rate is displayed in figure 3. Reasonable accuracy with the maximum difference of about 8% is obtained for both cases. The maximum discrepancy occurs at the dissipation and enstrophy peak, resulted from the stretching of the vortex filaments to fine scale during the transition process of the vortex pair. The plot of  $dK/dt$  also indicates that the ambient turbulence makes the instability of the vortex pair develop earlier.

#### Flow Visualisation

The evolution of the three-dimensional instabilities of the vortex pair is visualised by means of the isosurfaces of the second invariant of the velocity gradient tensor  $Q = -0.5u_{i,j}u_{j,i}$  (for details see [4]), as shown in figures 4 and 5. For the vortex pair in a quiescent background, it can be clearly seen from figure 4(a) that the short-wavelength instability develops. This instability leads to the distortion of the vortex pair into a sinusoidal shape with the wavelength of about unity (corresponding to the wavenumber of about 6). With time, the transverse secondary vortex develops, as displayed in figure 4(b). The sec-

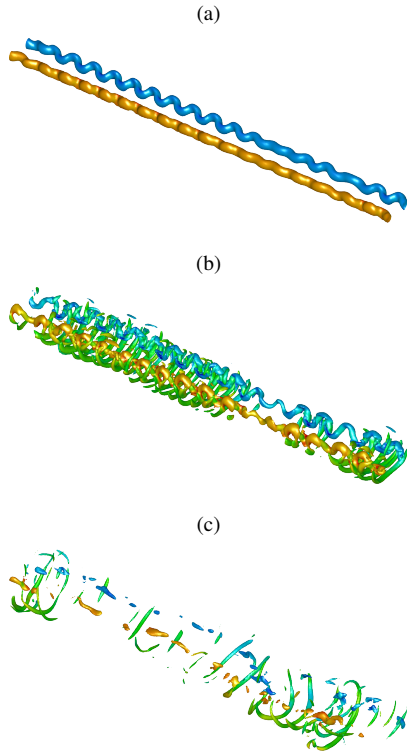


Figure 4. The coherent structures of the vortex pair in a quiescent background visualised by the isosurfaces of  $Q$ , coloured by  $\omega_x$ , at (a)  $t = 13$ , (b)  $t = 16$  and (c)  $t = 19$ .

ondary vortex accelerates the breakdown process by stretching the vortex pair along the axial direction leading to small-scale structures. Later, the turbulent vortex pair rapidly decays and disappears without the formation of a large-scale coherent structure (e.g. a vortex ring), as illustrated in figure 4(c).

Once the vortex pair is embedded in the moderate ambient turbulence ( $Tu = 7\%$ ), both the short- and long-wavelength instabilities seem to develop simultaneously (figure 5a). However, since the long-wavelength Crow mode dominates the flow (see the next subsection below), it brings the vortices close together causing the mutual interaction of the two vortices, as depicted in figure 5(b). At the locations of each mutual interaction, each vortex disconnects from the axial vortex and then reconnects with each other transforming the vortex pair into a series of vortex rings (figure 5c).

### Spectral Analysis

To investigate the evolution of the energy spectrum of each axial mode, a Fourier transform in the streamwise direction is performed. The axial wavenumber is  $\kappa_x = 2\pi m/L_x$  (where  $m = 1, \dots, nx/2$ ) and the corresponding wavelength is  $\lambda_x = 2\pi/\kappa_x$ . Figure 6 displays the axial modal kinetic energies at some selected times, while the evolution of the most amplified wavenumber is plotted in figure 7. In a quiescent background (figure 6a), the energy of each axial wavenumber is approximately the same at the beginning ( $t = 0$ ). This confirms that the magnitude of the random perturbation used is high enough to prevent the effect of the numerical error that excites only some particular modes. With time, the energy of each mode increases individually with different growth rates, resulting in different levels of energy during the breakdown process starting at  $t \approx 13$ . The mode that has the highest energy during this period is  $\kappa_x = 6.33$ , with the corresponding wavelength  $\lambda_x = 0.99$ . The evolution of this mode is illustrated in figure 7a.

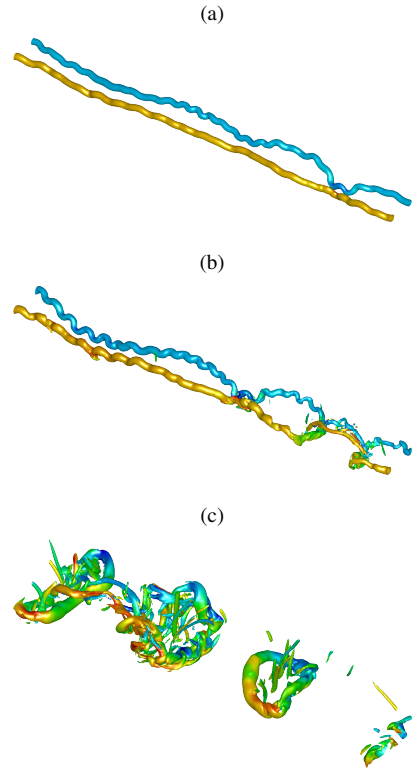


Figure 5. The coherent structures of the vortex pair in ambient turbulence with  $Tu = 7\%$  visualised by the isosurfaces of  $Q$ , coloured by  $\omega_x$ , at (a)  $t = 3.5$ , (b)  $t = 5$  and (c)  $t = 10$ .

The growth rate of this mode during the linear instability phase is  $\alpha = 0.5d(\ln E^*)/dt = 0.84$ . The values of the wavelength and growth rate found in this work agree reasonably well with those reported in the experiment [7] ( $\lambda_x = 0.77$ ,  $\alpha = 0.94 \pm 0.12$ ) and DNS simulations of Laporte & Corjon [5] ( $\lambda_x = 0.85 \pm 0.05$ ,  $\alpha = 0.96 \pm 0.3$ ) and Nomura *et al.* [9] ( $\lambda_x = 1.0$ ,  $\alpha = 0.83$ ).

In a turbulent ambient, the energy spectrum at  $t = 0$  is consistent with the Kolmogorov turbulence cascade, showing the transfer of energy from larger scales to smaller scales (figure 6b). Although the energy of each mode increases with different growth rates similar to the vortex pair in a quiescent background, the external turbulence alters the most amplified wavenumber to  $\kappa_x = 1.0$ , with the growth rate of 0.28 (figure 7b). It is of interest to note that the most dominant elliptic mode is still  $\kappa_x = 6.3$  during the linear instability phase (i.e. at  $t = 3.5$ ). Although the most amplified wavelength ( $\lambda_x = 6.28$ ) agrees very well with the Crow mode of Laporte & Corjon [5], the growth rate found in this work is about 2.5 times lower. This happens presumably because the initial energy of the vortex pair in the external turbulence is much higher (about  $6 \times 10^5$  times) than that in the quiescent background. If we further assume that the time spent during the transition process and the maximum energy that the flow can contain are independent of the initial energy, it can be implied that the growth rate of the Crow mode depends on the initial energy (in other words depending on the level of the turbulence intensity). Simulations with various levels of turbulence intensity are needed in order to support this assumption.

### Conclusions

The effect of the ambient turbulence with the intensity of 7% on the three-dimensional instabilities of a counter-rotating vortex pair is investigated via the use of direct numerical simulation. It is found that the external turbulence causes the earlier onset of

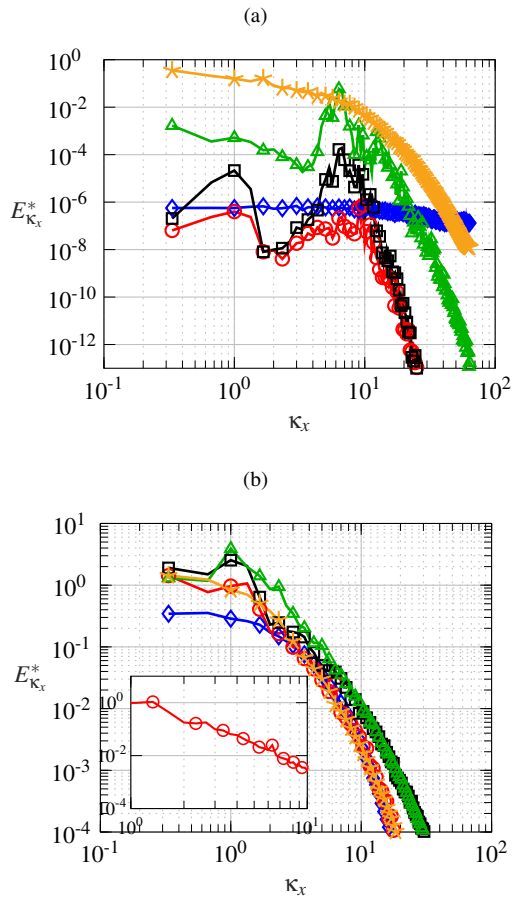


Figure 6. Axial modal energies for (a)  $Tu = 0$  at  $t = 0, 5, 9, 13, 22$  and (b)  $Tu = 7\%$  at  $t = 0, 3.5, 5, 10, 22$ . Symbols  $\diamond$ ,  $\circ$ ,  $\square$ ,  $\triangle$  and  $\star$  correspond to each time in ascending order.

the transition. Additionally, the most amplified mode of the vortex pair is altered from the elliptic mode ( $\kappa_x = 6.33$  for  $Tu = 0$ ) to the Crow mode ( $\kappa_x = 1.0$  for  $Tu = 7\%$ ). The breakdown due to the Crow mode introduces the mutual interaction of the two vortices, which leads to the reconnection of the vortex pair. This results in the appearance of a chain of vortex rings. In future work, the influence of various levels of turbulence intensity on the short- and long-wavelength instabilities will be investigated.

#### Acknowledgements

The authors gratefully acknowledge the financial support from Chiang Mai University and the use of HPC services of the Faculty of Engineering, Chiang Mai University.

#### References

- [1] Chevalier, H., Flight test studies of the formation and dissipation of trailing vortices, *J. Aircr.*, **10**, 1973, 14–18.
- [2] Crow, S. C., Stability theory for a pair of trailing vortices, *AIAA J.*, **8**, 1970, 2172–2179.
- [3] Gerz, T., Holzäpfel, F. & Darracq, D., Commercial aircraft wake vortices, *Prog. Aeosp. Sci.*, **38**, 2002, 181–208.
- [4] Jeong, J. & Hussain, F., On the identification of a vortex, *J. Fluid Mech.*, **285**, 1995, 69–94.
- [5] Laporte, F. & Corjon, A., Direct numerical simulations of the elliptic instability of a vortex pair, *Phys. Fluids*, **12**, 2000, 1016–1031.

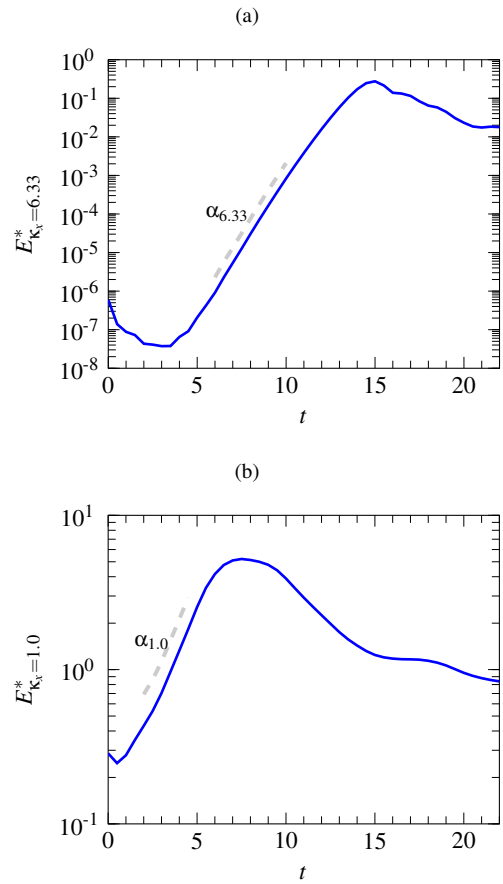


Figure 7. Evolution of the most amplified axial modal energy for (a)  $Tu = 0$  and (b)  $Tu = 7\%$ .

- [6] Leweke, T., Le Dizès, S. & Williamson, C. H. K., Dynamics and instabilities of vortex pairs, *Annu. Rev. Fluid Mech.*, **48**, 2016, 507–541.
- [7] Leweke, T. & Williamson, C. H. K., Cooperative elliptic instability of a vortex pair, *J. Fluid Mech.*, **360**, 1998, 85–119.
- [8] Mansour, N. N. & Wray, A. A., Decay of isotropic turbulence at low Reynolds number, *Phys. Fluids*, **6**, 1994, 808–814.
- [9] Nomura, K. K., Tsutsui, H., Mahoney, D. & Rottman, J. W., Short-wavelength instability and decay of a vortex pair in a stratified fluid, *J. Fluid Mech.*, **553**, 2006, 283–322.
- [10] Orlandi, P., Carnevale, G. F., Lele, S. K. & Shariff, K., Thermal perturbation of trailing vortices, *Eur. J. Mech. B-Fluids*, **20**, 2001, 511–524.
- [11] Proctor, F., Ahmad, N., Switzer, G. S. & Duparcmeur, F. M. L., Three-phased wake vortex decay, in *AIAA Atmospheric and Space Environments Conference*, Toronto, Canada, 2010.
- [12] Spalart, P. R., Airplane trailing vortices, *Annu. Rev. Fluid Mech.*, **30**, 1998, 107–138.
- [13] Switzer, G. F. & Proctor, F. H., Numerical study of wake vortex behavior in turbulent domains with ambient stratification, *AIAA Paper 2000-0755*, 2000.